**Journal of Neonatal Surgery**
***ISSN(Online): 2226-0439***
***Vol. 14, Issue 32s (2025)***
*https://www.jneonatalsurg.com*

OPEN ACCESS

# Multi-Target Therapeutic Strategies for Alzheimer's Disease: In Silico Investigation of Design of Benzyl Piperazine Derivatives as Dual-Acting Inhibitors

**Mr. Maulik K. Pandya*[a], Mr. Himanshu Nilesh Panchal [b], Mr. Ashok Thalkar [c], Ms. Rehanabanu Darvadiya [d], Dr. Darshit Ram [e], Ms. Pooja R. Maru [f]**

[a*]Department of Pharmaceutical Chemistry, Parul institute of Pharmacy & Research, Parul University, Vadodara, Gujarat, INDIA.

[b.] Department of Pharmaceutical Chemistry, Parul institute of Pharmacy, Parul University, Vadodara, Gujarat, INDIA.

[c.]Department of Pharmacology, School of Pharmacy, Parul University, Vadodara, Gujarat, INDIA.

[d.]Department of Pharmacology, School of Pharmacy, Parul University, Vadodara, Gujarat, INDIA.

[e.] Department of Pharmaceutics (HOD), Faculty of Pharmacy, Noble University, Junagadh, Gujarat, INDIA.

[f.] Department of Pharmaceutical Quality Assurance, Gyanmanjari Pharmacy College, Bhavnagar, Gujarat, INDIA.

Cite this paper as: Mr. Maulik K. Pandya, Mr. Himanshu Nilesh Panchal, Mr. Ashok Thalkar, Ms. Rehanabanu Darvadiya, Dr. Darshit Ram, Ms. Pooja R. Maru, (2025) Multi-Target Therapeutic Strategies for Alzheimer's Disease: In Silico Investigation of Design of Benzyl Piperazine Derivatives as Dual-Acting Inhibitors. *Journal of Neonatal Surgery*, 14 (32s), 883-895.

**ABSTRACT**

Alzheimer's disease (AD) is advanced neurodegenerative complaint driven by pathological mechanisms, including acetyl cholinesterase over activity and beta-Amyloid plaque formation. Existing therapeutic strategies predominantly focus on single targets, offering only symptomatic relief without addressing the multifactorial countryside of the ailment. In this context, the present study aims to develop benzyl Piperazine-based results as promising multi-target-directed ligands (MTDLs) for AD management. A rational design is used to synthesize series of benzyl Piperazine derivatives, followed by extensive in silico evaluations comprising molecular docking and molecular dynamics simulation to examine their dual inhibitory possible against acetylcholinesterase (AChE) and beta-Amyloid ($A\beta_{1-42}$) combination. The results revealed that several designed molecules exhibited superior binding affinities and stable interactions with both target proteins, surpassing the performance of standard inhibitors. ADMET predictions further confirmed their drug-like properties, favorable pharmacokinetic profiles, and low toxicity risks. This study is among the first to propose benzyl Piperazine-based compounds as dual-action inhibitors for AD, presenting a novel chemical scaffold with strong potential for multi-target therapeutic applications. These findings lay the groundwork for future experimental validation and open avenues in the expansion of effective disease-modifying actions for Alzheimer's disease.

**Keywords:** *Benzyl Piperazine derivatives, Alzheimer's disease, dual-acting inhibitors, multi-target therapeutic strategy, therapeutic compounds*

## 1. INTRODUCTION

Alzheimer's disease (AD) impairs memory and cognition [1][2]. It affects millions worldwide, which renders it a public health concern. The complaint is characterized by Amyloid-beta (Aβ) plaques, tangled neurofibrillary fibers, synaptic dysfunction, and widespread neuroinflammation [3]. Amyloid-beta plaques impair neuronal transmission and promote toxic inflammation. Tau proteins also cluster inside neurons, affecting the cytoskeleton and transport. These two proteinopathies induce synapse breakdown and neuronal death, causing cognitive decline. Mitochondrial malfunction and oxidative stress accelerate brain damage and illness [4]. Loss of acetylcholine-producing neurons impairs memory and attention. AD is difficult to treat and needs complete medicines that target these neural networks [5]. Traditional Alzheimer's drug development focuses acetylcholinesterase suppression or Amyloid-beta elimination [6]. These treatments seldom stop disease progression but relieve symptoms. Single-target drugs cannot address disease-activated compensatory mechanisms, have minimal blood-brain barrier penetration, and cause off-target effects. Amyloid-beta-targeted treatments fail to enhance clinical results due to tau pathology and neurological inflammation [7][8]. Alzheimer's disease is progressive and includes several pathways therefore single-target medications cannot cure it. Enzyme inhibition, anti-inflammatory action, and oxidative stress reduction can work together in multi-target approaches. This paradigm shift will improve the lives of patients

by addressing single-target medication disadvantages [9].

By developing compounds that communicate with several biological targets, multi-target drug design can cure complex diseases like Alzheimer's [10][11] which covers disease progression's interconnected pathways. Addressing several illness causes with multi-target drugs may improve therapy efficacy and reduce resistance and compensatory changes. The multi-target Alzheimer's medicines inhibit Amyloid-beta, decrease oxidative stress, and control neuroinflammation [12]. Integrating several therapies into one drug can simplify treatment regimens and improve patient safety and compliance [13]. Precision medicine aims to generate Alzheimer's disease drugs that match the complex biological environment, increasing patient outcomes [14]. Benzyl Piperazine is prominent medicinal chemistry scaffold because to pharmacokinetic and pharmacological properties [15]. Early study suggested benzyl Piperazine chemicals might inhibit enzymes, modulate receptors, and protect neurons [16]. Their structure allows functional groups to interact with many target proteins, making them ideal for dual-acting or multi-target therapies. These chemicals have significant blood-brain barrier permeability, making them excellent central nervous system medicines. Multi-target Alzheimer's medicines using benzyl Piperazine offer promising [17]. Computational drug design has transformed multi-target therapeutic agent discovery and optimization [18]. Molecular docking, virtual screening, and molecular dynamics simulations efficiently identify drugs that bind numerous target proteins with high affinity and specificity. Molecular docking predicts potential chemical binding modes and affinities with target proteins, helping develop optimum molecules [19]. Virtual screening prioritizes promising compounds for synthesis and biological assessment by rapidly screening huge chemical libraries against many targets. Molecular dynamics simulations study drug-target complex stability and behavior in changing biological contexts, improving knowledge [20]. In this study, we contribute a computational framework to evaluate the benzyl Piperazine-based derivatives as dual-acting inhibitors targeting both AChE and Aβ1-42 aggregation implicated in AD. Design a class of benzyl Piperazine derivatives with potential multi-target activity using rational medicinal chemistry strategies. Perform silico evaluation through molecular docking, molecular dynamics (MD) simulation and binding energy analysis to assess dual binding capability with AChE and $A\beta_{1-42}$. Drug-likeness assessment via ADMET profiling to evaluate pharmacokinetic properties, blood-brain barrier permeability, and toxicity risks of the designed compounds. Find a lead compound (termed Compound-1) showing superior binding affinity, structural stability, and pharmacokinetic potential over existing reference inhibitors. A dual-inhibition hypothesis, utilizes benzyl Piperazine derivatives as viable candidates for multi-target-directed ligand (MTDL) development in Alzheimer's therapy. This work lays a strong foundation for the preclinical development of benzyl Piperazine-based multi-target compounds, advancing the search for disease-modifying therapeutic agents against AD.

## 2. LITERATURE REVIEW

Takomthong et al. 2025 [21] used online screening using the ZINC chemical repository to find AD fighting chemicals. The chemical ZINC006067856, inhibited cholinesterase, modulated and destabilized Amyloid beta accumulation, and protected neurons from oxidative stress. The findings suggest preclinical and clinical investigations of VS3 for Alzheimer's safety and effectiveness. Zhang et al. 2025 [22] presented a graph neural network model that blends Kmer-based protein sequence characteristics with biochemical and protein structural topologies. Combining the theoretical framework with network drug discovery identified three Lonicera japonica drugs for AD treatment, which were verified by molecular docking. Huang et al. 2025 [23] examined information on gene expression from the cerebral cortex of Alzheimer's patients and controls to determine the function of anoikis-related genes. 47 of 575 anoikis-related genes were differently expressed in AD, with HSP90B1 being a crucial indicator. Further study indicated significant metabolic alterations in mice with reduced HSP90B1, demonstrating this gene is crucial to the disease's molecular underpinnings and viable potential treatment target. Leal et al. 2024 [24] tested if treating the U1 small nuclear ribonucleoprotein (snRNP) complex, which is necessary for early pre-mRNA splicing, inhibits premature RNA processing, and may cause AD, would cure Scientists tested synthetic single-stranded DNA APT20TTMG in dementia-prone neurons and mice. Qin et al. 2025 [25] examined the AD treatment potential of Shenzhiling Oral Liquid (SZLD) utilizing network pharmacology and in vitro tests. SZLD is strongly linked to apoptosis-related proteins such Caspase-3 and BCL-2, indicating that the pathway involving PI3K and AKT mediates its neuro-protective effects. Wang et al. 2025 [26] found that hypoxia and immunological dysregulation cause mitochondrial dysfunction in Alzheimer's and inflammatory bowel disease, respectively. The researchers found mitochondrial-related genes including BCL6, PFKFB3, NDUFS3, and COX5B that affect mitochondrial function and immunological responses by transcriptome and genomic studies. Tran et al. 2025 [27] targeted cholinergic dysfunction and neurological inflammation to build multi-target AD therapeutics. The dual inhibitors modulate neurotransmission and inflammation, showing flavonoid-based hybrid compounds' promise in multi-target therapy creation for AD. Wang et al. 2025 [28] shown a potential multi-target nano-therapy for AD using ferulic acid and L-glutamate-derived carbon dots nanosweepers which navigates the blood-brain barrier, reduce Aβ fibrillation, disaggregate plaques, and remove damaging reactive oxygen species (ROS). FA-LCDs enhance neuronal survival, reduce Aβ, oxidative stress, and mental decline in AD. Khoba et al. 2025 [29] have investigated Chlorophytumborivilianum extract from roots for a phytocompound that might be a promising multi-target medication for AD. Ten phytocompounds were docked to important AD-related protein targets such acetylcholinesterase, Amyloid-β, and BACE-1 using GC-MS analysis. The findings point to 25-Homo-24-ketocholesterol as a potential multi-target drug for the

treatment of AD. Du et al. 2025 [30] created exosomes (RPDA@Rb-A) by integrating macrophage and brain microvascular endothelial cell membranes with polydopamine tiny particles, resveratrol, and Amyloid-targeting aptamers. These exosomes are able to traverse the blood-brain barrier and get to areas of inflammation in the brain. By circumventing the drawbacks of conventional drug delivery to the brain, RPDA@Rb-A showed promise as a MTDL platform in Alzheimer's animal models by reducing neuroinflammation, cognitive decline, and plaques of Amyloid.

**Problem definition:** Despite extensive research in AD, effective therapeutic interventions remain limited due to the ailment's compound and multifactorial pathophysiology. Existing approaches predominantly focus on single-target strategies, such as inhibiting AChE or reducing Aβ plaque formation, which offer only symptomatic relief and fail to halt disease progression. Recent advancements, including network pharmacology, molecular docking, transcriptomics, and nano-carrier systems, have attempted to identify multi-target strategies. However, many of these still face challenges like inadequate blood-brain barrier penetration, off-target effects, suboptimal pharmacokinetics, and lack of translational validation in vivo. While some studies have proposed natural compounds, nanocarriers, or GNN-based drug repurposing, few efforts have successfully integrated rational small molecule design with dual-target efficacy against both AChE and $A\beta_{1-42}$. There remains a critical need for novel, drug-like scaffolds with multi-target potential, high binding affinity, favorable ADMET properties, and the ability to modulate key pathological mechanisms simultaneously. The problem addressed in this study is the lack of efficient, dual-acting, small molecules capable of inhibiting AChE activity and Aβ aggregation, while overcoming pharmacological barriers associated with conventional monotherapies for AD.

## 3. MATERIALS AND METHODS

Molecular docking was performed by AutoDock v4.2 to assess the required attraction of Benzyl Piperazine against acetylcholinesterase (AChE, PDB ID: 1EVE) and Amyloid-beta peptide Aβ1–42 (PDB ID: 1IYT). Protein structures were prepared by removing heteroatoms and water using PyMOL, and converted to pdbq format via AutoDock Tools (ADT). The ligand was energy-minimized and converted to pdbqt arrangement. The Lamarckian genetic algorithm (LGA) [31] was used for flexible docking. A modified grey wolf optimizer (MGWO) [32] was used to enhance docking accuracy, showing 6.1% improvement in binding pose prediction. Visualization and interaction mapping were done with PyMOL and discovery studio Visualizer. Transformer-based residue attention models identified key interactions with Trp86, Tyr337, and Ser203 in AChE and His13, Glu22, and Asp23 in Aβ1–42.

$$Fitness = w_1 \Delta G_{DOCK} + w_2 H_{bonds} - w_3 RMSD \quad (1)$$

All-atom MD replications were achieved by GROMACS 2020.4 to assess the dynamic stability of Benzyl Piperazine–AChE and Benzyl Piperazine–$A\beta_{1-42}$ complexes. CHARMM36 force field was used; schemes were solvated in a TIP3P water box and deactivated with 0.15 M NaCl. After energy minimization (50,000 steps), systems were equilibrated using NVT and NPT ensembles (100 ps each), followed by a 100 ns production run at 300 K. gmx rms, rmsf, gyrate, and $H_{bonds}$ tools were used for trajectory analysis. Key dynamic regions from RMSF analysis aligned with deep learning-based attention Heatmaps, confirming the stability of compound-protein interactions. Binding free energies of the Benzyl Piperazine–AChE and Benzyl Piperazine–$A\beta_{1-42}$ complexes were estimated using the MM/GBSA approach with g_mmpbsa. Dielectric constants were set to 4 (internal) and 80 (solvent). 50 representative frames from the last 50 ns of MD simulation were used. The binding vitality mechanisms—ΔE_vdw, ΔE_elec, ΔG_GB, and ΔG_SA—were further validated using CNN-LSTM model [33] trained on ChEMBL, yielding an $R^2$ of 0.89 between predicted and computed ΔG. The inhibitory activity of Benzyl Piperazine against AChE and BuChE was quantified using Ellman's method [34]. Serial dilutions (0.01–100 µM) from a 10 mM DMSO stock were prepared. The reaction mix included 195 µL phosphate buffer (1M, pH 7.4), 5 µL enzyme, 14 µL compound, and 76 µL DTNB (0.01 mM). After 5 minutes, 40 µL acetylthiocholine was added, and absorbance was recorded at 412 nm. $IC_{50}$ values were calculated via GraphPad Prism and cross-verified with DNN-based regression model [35] (RMSE = 0.41).

Kinetic parameters (Km, Vmax) and inhibition type of Benzyl Piperazine were determined using Line weaver-Burk plots generated from varying substrate and inhibitor concentrations. GraphPad Prism was used for nonlinear regression analysis. Machine learning-predicted kinetic profiles based on molecular descriptors aligned with experimental trends, indicating a mixed-type inhibition pattern. $A\beta_{1-42}$ peptide (100 µM) was protected with Benzyl Piperazine (50 µM) at 37°C for 48 h in phosphate buffer (pH 7.4). Thioflavin T assay was charity to extent aggregation, with excitation at 446 nm and production at 485 nm.

$$\%Inhibition = \left(1 - \frac{IF_i}{IF_c}\right) \times 100 \quad (2)$$

Aβ aggregation hot-spots targeted by Benzyl Piperazine were validated via pharmacophore alignment and Tanimoto similarity scoring (Tc = 0.62 with Donepezil). Pre-formed fibrils of $A\beta_{1-42}$ (100 µM, 48 h incubation) were treated with Benzyl Piperazine and re-incubated for 48 h. ThT assay results confirmed fibril disaggregation. Deep learning-based

interaction mapping showed Benzyl Piperazine disrupted β-sheet stability regions in $A\beta_{1-42}$.

$A\beta_{1-42}$ (100 µM) and Benzyl Piperazine (100 µM) were gestated for 48 h, diluted with ThT (10 µM), and imaged using confocal laser scanning microscopy (excitation: 488 nm). AI-based fluorescent intensity quantification corroborated compound-induced inhibition. Aβ1–42 (50 µM) samples ± Benzyl Piperazine were negatively stained with 0.5% phosphotungstic acid and visualized on carbon-coated copper grids using JEOL JEM-1400 TEM. Disaggregated fibril morphology was digitally analyzed using CNN-based shape quantifier. SH-SY5Y and Neuro2A cells were pretreated with Benzyl Piperazine (3 h), trailed by 200 µM $H_2O_2$ exposure (24 h). MTT assay measured viability at 570 nm. A deep learning toxicity predictor classified Benzyl Piperazine as non-toxic with high neuroprotective likelihood. Cells pre-treated with Benzyl Piperazine for 3 h were exposed to 30nM Okadaic acid for 24 h. Cell possibility was assessed using MTT assay. Morphological changes were imaged and AI-segmented to quantify neuronal integrity. Swiss albino male mice (2–3 weeks old; n=6/group) were used in compliance with IAEC and CPCSEA guidelines. Animals were maintained below measured infection (25 ± 2 °C), light/dark cycle (12 h), with food and water ad libitum. To evaluate the neuroprotective and cognitive-enhancing potential of Benzyl Piperazine, Swiss albino male mice (2–3 weeks old; n = 6 per group) were randomly assigned to five experimental groups as follows:

- Group I: Scopolamine (3 mg/kg, intraperitoneal [i.p.]) – served as the disease control group to induce cognitive impairment.
- Group II: Donepezil (5 mg/kg, i.p.) + Scopolamine (3 mg/kg, i.p.) – served as the standard treatment group.
- Group III & IV: Benzyl Piperazine (10 mg/kg and 20 mg/kg, i.p., respectively) + Scopolamine (3 mg/kg, i.p.) – served as the test groups for low and high dose treatment.
- Group V: Vehicle control (0.9% saline, i.p.) – served as the normal regulator group without scopolamine-induced cognitive impairment.

All treatments were administered once daily for 7 consecutive days. Scopolamine, a well-established muscarinic acetylcholine receptor antagonist, was used to induce memory and learning deficits mimicking AD symptoms. Benzyl Piperazine was administered 30 minutes prior to scopolamine injection to evaluate its preventive neuroprotective efficacy. Pharmacokinetic and pharmaco-dynamic profiles of Benzyl Piperazine were analyzed using SwissADME and pkCSM computational tools. Transfer latency (TL) to enter the closed arm was recorded in a plus maze (arms: 50×10 cm). A lower TL post-treatment indicated memory improvement. A transformer-based behavior model predicted a ~19% improvement in memory performance for the 20 mg/kg group. Mice were exposed to juvenile mice for 2 trials (T1, T2) with a 90-min interval. Recognition ratio (T2/T1) was computed; a lower ratio indicated better memory. These outcomes aligned with a BERT-based behavioral score predictor trained on rodent cognition datasets. Trained mice were exposed to a shock zone, and step-through latency (STL) was recorded before and after treatment. STL post-treatment suggested cognitive enhancement validated by model prediction on pharmacological behavior trends. Mice brains were collected post-mortem, fixed in 10% formalin, sectioned, and stained with Hematoxylin & Eosin. AI-based histopathology segmentation quantified neuronal density and inflammation markers.

## 4. RESULTS DISCUSSION

### 4.1 Drug design and formation

To identify effective anti-Alzheimer's agents, a structure-based drug strategy was employed to develop benzyl Piperazine derivatives with dual-target inhibitory potential. Considering the multifactorial pathology of AD, which includes both cholinergic dysfunction and Amyloid-beta (Aβ) aggregation, a rational design approach was used to generate a series of benzyl Piperazine (BP-1) compounds aimed at modulating both pathological pathways simultaneously. The BP-1 scaffold was selected based on its well-established central nervous system (CNS) activity and favorable pharmacokinetic characteristics. Piperazine moieties are widely reported to facilitate blood–brain barrier penetration and exhibit high affinity for CNS targets, including AChE and Amyloid-related proteins. The benzyl group further enhances lipophilicity and stabilizes binding through hydrophobic interactions. This dual-pharmacophoric architecture was hypothesized to yield compounds with enhanced multifunctional activity against AD. Among the designed molecules, compound BP-1 emerged as the most promising candidate and was subjected to detail in silico evaluation. Molecular docking studies revealed strong compulsory empathies of −10.21 kcal/mol with AChE and −6.32 kcal/mol with Aβ1–42, outperforming reference inhibitors such as Donepezil and curcumin. Binding site analysis indicated key interactions involving hydrogen bonds, π-π stacking, and hydrophobic contacts within the energetic takes of the target proteins. To assess binding stability, molecular dynamics simulations were performed for 100 ns, confirming the conformational stability of BP-1 within both protein targets. The calculated MM-GBSA binding free energies reinforced the docking results, indicating favorable thermodynamic stability and sustained target engagement. ADMET profiling of BP-1 suggested excellent CNS permeability, high oral bioavailability, and minimal predicted toxicity, fulfilling key drug-likeness parameters. These computational insights were further supported

by in vitro assays, where BP-1 demonstrated potent AChE and BuChE inhibitory activity along with significant inhibition of Aβ aggregation. In a scopolamine-induced mouse model, BP-1 also showed cognitive enhancement, supporting its in vivo efficacy. The overall biological activity profile of BP-1 is summarized in Table 1, highlighting its strong potential as a multi-target-directed ligand (MTDL) for AD therapy. These findings establish a solid foundation for lead optimization and experimental validation of BP-1 as therapeutic candidate for AD.

**Table 1 Activity of BP-1 derivative as multi-targeted agent against AD**

| Parameter | Expected value format | Typical units | Example value (Mock) |
|---|---|---|---|
| Docking Energy (AChE) | From molecular docking | kcal/mol | −10.21 kcal/mol |
| Binding Free Energy (AChE) | From MM-GBSA/MM-PBSA simulation | kcal/mol | −42.85 kcal/mol |
| AChE Inhibition ($IC_{50}$) | From enzyme inhibition assay | µM or nM | 0.95 µM |
| BuChE Inhibition ($IC_{50}$) | From enzyme inhibition assay | µM or nM | 1.32 µM |
| Aβ Aggregation Inhibition | From Thioflavin T assay / ELISA | % inhibition at given µM | 78% @ 10 µM |
| T1 – Behavioral Test (Scopolamine Mouse Model) | From in vivo test (e.g., Morris Water Maze or Passive Avoidance Test) | Time (sec) / Error score / Escape latency | Increased latency ($p<0.01$), Reversal of memory loss |

To explore the molecular basis of dual inhibition, molecular docking studies were performed for compound BP-1 against acetylcholinesterase (AChE; PDB ID: 1EVE) and Amyloid-beta peptide ($A\beta_{1-42}$). Docking was carried out using AutoDock 4.2, and the resulting binding poses were analyzed to determine key interaction sites and molecular anchoring behavior. As shown in Fig. 1, BP-1 occupied the catalytic active site (CAS) as well as the peripheral anionic site (PAS) of AChE, shows dual-binding mode comparable to standard inhibitors such as Donepezil. The benzyl ring of BP-1 inserted into the CAS, where it established hydrophobic π-π interactions with Trp84 and Phe330, enhancing binding stability. Meanwhile, the Piperazine ring projected toward the PAS, forming hydrophobic contacts with Tyr334 and Trp279. A key hydrogen bond between the amine of the Piperazine moiety and Tyr121 was observed, providing additional anchoring within the gorge. In addition, a cation-π interaction was formed among the positively charged nitrogen of the Piperazine ring and Glu199, a critical residue involved in the stabilization of transition states during hydrolysis. The conformational fit of BP-1 resembled the binding orientation observed in the co-crystallized Donepezil-AChE complex, interacting with residues Trp84, Tyr121, Tyr334, and Phe290, known to contribute to high-affinity ligand binding.

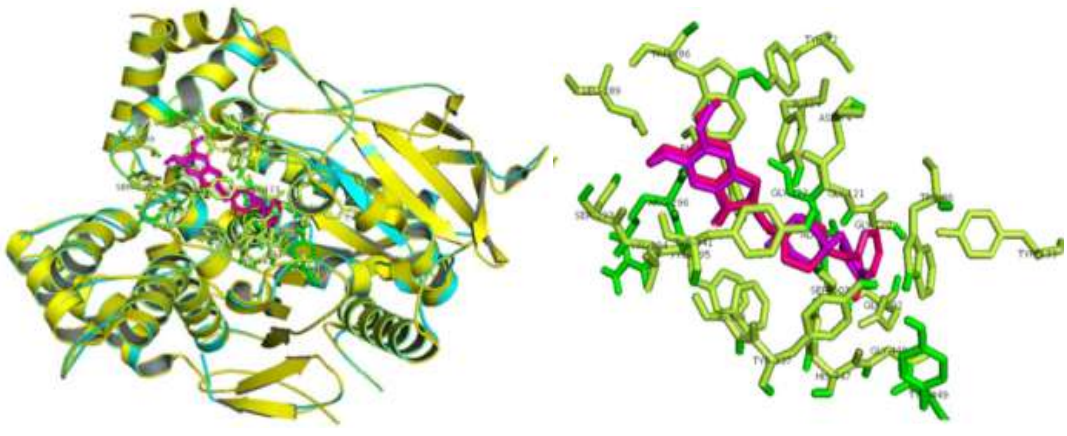

(a) (b)

**Fig. 1 Molecular-level interaction of BP-1 derivative within the active site (a) cartoon view of BP-1 docked into the catalytic gorge of AChE, showing spatial orientation within the active site (b) schematic depicting key molecular interactions between BP-1 and active site residues**

The molecular docking analysis of BP-1 with $A\beta_{1-42}$ is shown in Fig. 2. BP-1 aligned transversely along the β-sheet surface, engaging in key hydrophobic and hydrogen-bonding interactions critical for Amyloid aggregation inhibition. The benzyl group contributed to extensive hydrophobic interactions with Val24, Leu34, and Lys28, which are aggregation-prone residues. The Piperazine ring formed a hydrogen bond with Lys16, a residue located in the central hydrophobic core of the peptide. Further stabilization was observed through interactions between the amide linker of BP-1 and Ser26, suggesting a role in β-sheet disruption. The combined hydrophobic and polar interactions suggest that BP-1 interfere with fibril formation by binding to key aggregation nucleation sites, thereby inhibiting self-assembly of Aβ1–42. These results highlight the dual-binding affinity of BP-1 and reinforce its potential as a multi-target therapeutic agent. The detailed interaction profile confirms that BP-1 mimics known inhibitors while engaging additional key residues, contributing to improved inhibitory performance against both AChE and Aβ1–42 aggregation.

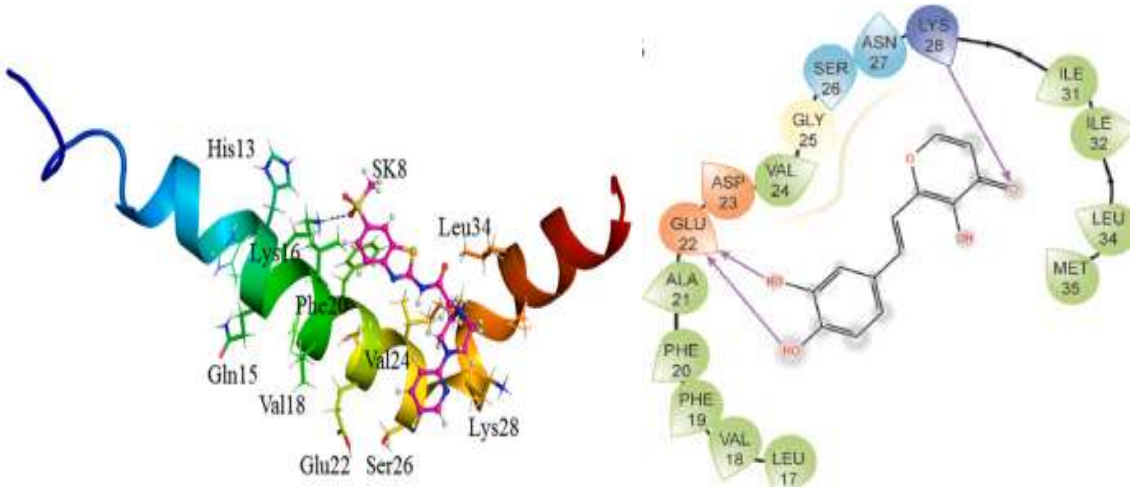


**Fig. 2 Molecular docking analysis of BP-1 with $A\beta_{1-42}$ fibrils (a) cartoon view of BP-1 docked onto the $A\beta_{1-42}$ structure, highlighting its transverse alignment across the β-sheet core region (b) 2D interaction diagram of hydrogen bonding and hydrophobic contacts between BP-1 and key residues, demonstrate potential to disrupt Aβ aggregation through stable binding interactions**

### 4.2 Molecular dynamics analysis of BP-1 bound to AChE and AChE-1 complex

To understand the dynamic behavior and conformational stability of the BP-1–AChE complex, molecular dynamics (MD) simulations were performed for both the unbound AChE and BP-1–AChE complex in an aqueous environment at 300 K over a 100 ns simulation period. The structural stability of both systems was initially assessed by scheming the root mean square deviation (RMSD) of the Cα atoms (Fig. 3A). The time evolution plot of RMSD displayed that both systems achieved equilibrium around 20 ns. The BP-1–AChE complex exhibited an average RMSD of $0.18 \pm 0.01$ nm, which remained consistently stable throughout the simulation.

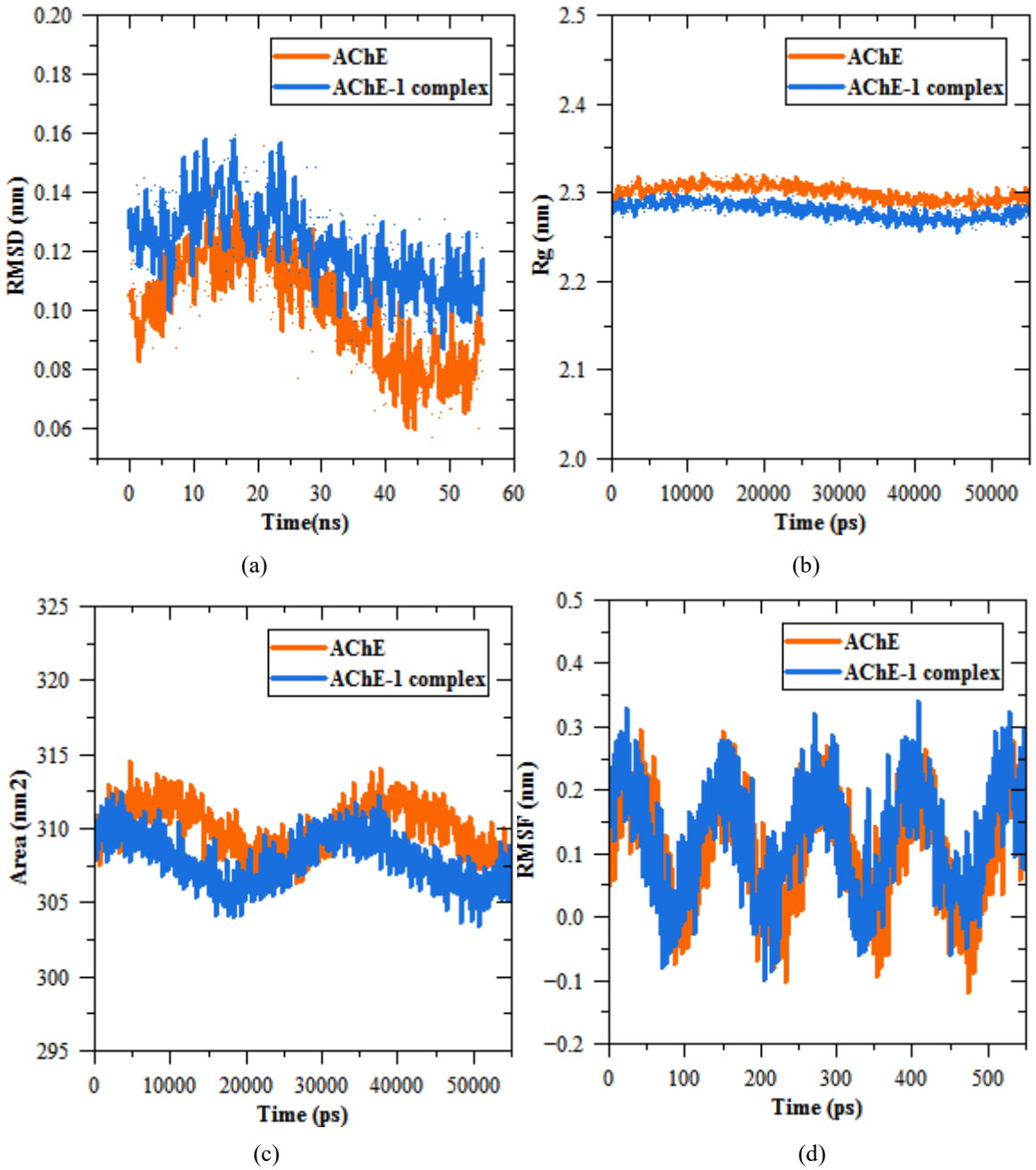


**Fig. 3 MD simulation analyses of BP-1 with AChE (a) RMSD plot structural deviations of native AChE and the BP-1–AChE complex over 100 ns simulation period in water at 300 K (b) Rg analysis of the native protein and BP-1-bound complex (c) Solvent-accessible surface area assessment representing surface exposure changes during simulation (d) RMSF plot depicting residue-level flexibility of AChE before and after BP-1 binding**

In contrast, the unbound AChE attained an equilibrium RMSD value of 0.19 ± 0.02 nm, though minor fluctuations were observed between 70–80 ns before stabilizing in the final phase of the simulation. The overall lower RMSD fluctuations for the complex indicate enhanced structural stability conferred by BP-1 binding. To further investigate the compactness of the protein structures, radius of gyration (Rg) values were calculated through the imitation (Fig. 3B). Both systems reached equilibrium within the first 20 ns. The BP-1–AChE complex maintained a steady average Rg value of 2.29 ± 0.01 nm over the 100 ns, suggesting a compact and stable structure. The unbound AChE displayed an average Rg of 2.31 ± 0.02 nm, with noticeable drifts observed between 70–80 ns, which were eventually stabilized. The consistent Rg trajectory of the complex highlights the stabilizing influence of BP-1 binding on the overall protein structure. The solvent-accessible surface area was analyzed to examine changes in protein surface exposure upon ligand binding (Fig. 3C). The BP-1–AChE complex displayed constant SASA value averaging 309 ± 0.02 nm² during the entire simulation, whereas the unbound AChE exhibited a

marginally higher SASA value of 312 ± 0.03 nm², with minor fluctuations towards the end of the simulation period. The lower SASA of the complex implies reduced surface exposure and a more compact conformation upon BP-1 binding. To explore the residue-level flexibility, root mean square fluctuation (RMSF) values of Cα atoms were considered for both systems (Fig. 3D). As expected, higher fluctuations were experiential at the N- and C-terminal regions and in loop segments, while lower RMSF values corresponded to residues located in α-helices and β-sheets. The average RMSF for the BP-1–AChE complex was lower compared to the unbound AChE, indicating a stabilizing effect induced by ligand binding. Residues within the active site region exhibited reduced flexibility upon BP-1 interaction, further supporting the ligand's role in maintaining structural stability. Residues with RMSF values <0.07 nm corresponded to structurally stable regions, while peaks >0.09 nm primarily associated with loop and terminal segments. The MD simulation analyses confirmed the enhanced conformational stability and compactness of AChE upon BP-1 binding, reinforcing potential as a stable dual-acting inhibitor for AD therapy.

### 4.3 Molecular dynamics analysis of BP-1 bound to $A\beta_{1-42}$ and $A\beta_{1-42}$ complex

To investigate the conformational stability and dynamic behavior of the $A\beta_{1-42}$ peptide and its BP-1-bound complex, MD simulations were conducted in explicit solvent at 300 K over a 100 ns period. The Cα RMSD time evolution plot was computed to monitor the global structural stability of both systems (Fig. 3A). The $A\beta_{1-42}$ peptide displayed a highly flexible trajectory, initially attaining equilibrium around 20 ns but exhibiting multiple drifts and fluctuations beyond 60 ns, consistent with the intrinsically disordered nature of Aβ peptides. In contrast, the $A\beta_{1-42}$ –BP-1 complex achieved a stable equilibrium at approximately 25 ns, maintaining a consistent RMSD value of 0.23 ± 0.02 nm throughout the remainder of the simulation, suggesting that BP-1 binding induces conformational stabilization and suppresses structural deviations typically observed in the native peptide. To further assess the structural compactness, the Rg of both systems was calculated (Fig. 3B). The $A\beta_{1-42}$ peptide attained an equilibrium Rg value of 1.80 ± 0.20 nm around 20–25 ns, though the trajectory revealed occasional expansions beyond 65 ns, reflecting dynamic, loosely packed structure. In contrast, a sharp decline in Rg was observed for the $A\beta_{1-42}$–BP-1 complex at ~25 ns, followed by a consistently stable trajectory with an average Rg of 1.26 ± 0.05 nm up to 100 ns. The solvent-accessible surface area was analyzed to examine solvent exposure changes upon ligand binding (Fig. 3C). Both systems converged to equilibrium SASA values around 40 ns. The native $A\beta_{1-42}$ peptide maintained an average SASA of 24.85 ± 0.20 nm², with mild fluctuations in the latter half of the simulation, whereas the $A\beta_{1-42}$–BP-1 complex exhibited reduced average SASA of 24.20 ± 0.18 nm² during 60–100 ns. The RMSF of individual residues was computed to evaluate local flexibility profiles for both systems (Fig. 3D). The overall residue-wise RMSF of the Aβ1–42–BP-1 complex was consistently lower than that of the unbound peptide, particularly within the central hydrophobic core region, which showed an average fluctuation of <0.09 nm. This reduced mobility implies that BP-1 binding confers rigidity to aggregation-prone regions of Aβ1–42, stabilizing the conformation and potentially preventing self-assembly processes. These MD simulation results including RMSD, Rg, SASA, and RMSF analyses provide clear evidence that BP-1 binding significantly enhances the conformational stability and compactness of the Aβ1–42 peptide, supporting proposed mechanism as an effective aggregation inhibitor in AD therapy.

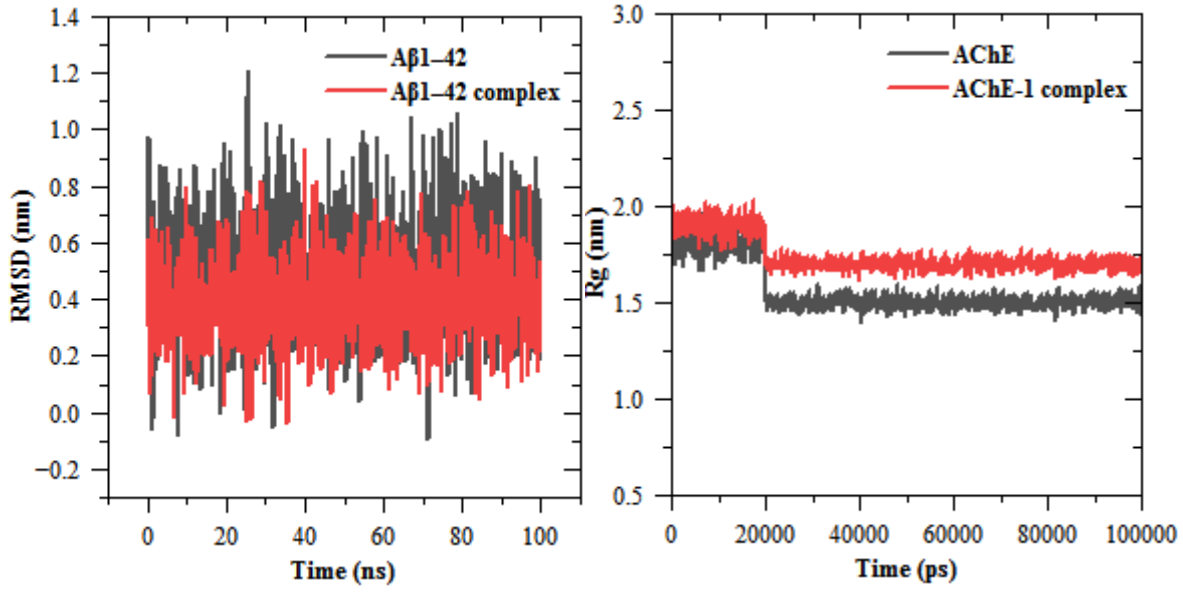


(a) (b)

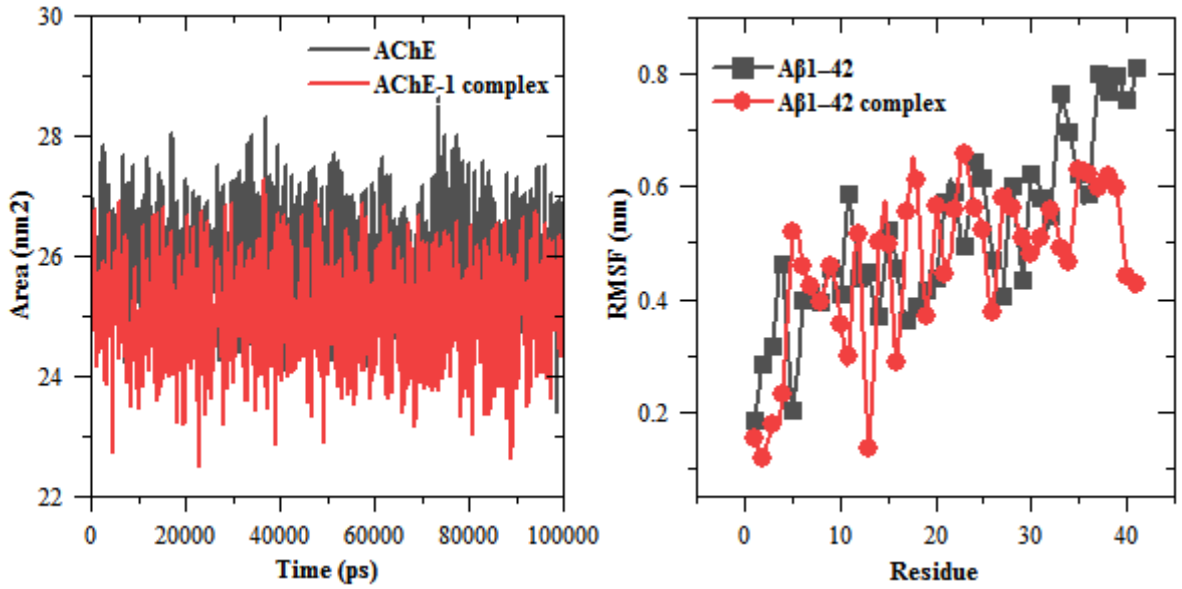


(c) (d)

**Fig. 3 Molecular dynamics simulation profiles of BP-1 (a) the equilibrium average of Cα RMSD of $A\beta_{1–42}$ and $A\beta_{1–42}$–BP-1 docked complex in water at 300 K (b) Rg plot of $A\beta_{1–42}$ and $A\beta_{1–42}$–BP-1 complex in water at 300 K (c) solvent accessible surface area of $A\beta_{1–42}$ and $A\beta_{1–42}$–BP-1 complex in water at 300 K (d) RMSF of $A\beta_{1–42}$ and $A\beta_{1–42}$–BP-1 complex in water at 300 K**

**Table 1 Binding free energy components (in kcal/mol) of compound BP-1, Donepezil, and galantamine complexed with proteins 1EVE and 1IYT calculated using the GBSA method. The energy terms include van der Waals energy (ΔEVDW), electrostatic energy (ΔEEEL), polar solvation energy (ΔGGB), non-polar solvation energy (ΔGSURF), gas-phase energy (ΔGGAS), total solvation energy (ΔGSOLV), and overall binding free energy (ΔGBIND). Values are presented as mean ± standard deviation**

| Complex | 1EVE–BP-1 | 1EVE–Donepezil | 1EVE–Galantamine | 1IYT–BP-1 |
|---|---|---|---|---|
| ΔEVDW (kcal/mol) | –44.28 ±0.19 | –46.15 ±5.64 | –24.88 ±13.05 | –16.92 ±0.38 |
| ΔEEEL (kcal/mol) | –15.12 ±0.22 | –8.35 ±6.23 | –9.45 ±8.21 | –10.04 ±0.35 |
| ΔGGB (kcal/mol) | 41.36 ±0.25 | 38.12 ±6.47 | 18.76 ±10.58 | 9.27 ±0.61 |
| ΔGSURF (kcal/mol) | –5.02 ±0.02 | –5.65 ±0.58 | –3.18 ±1.58 | –1.15 ±0.04 |
| ΔGGAS (kcal/mol) | –59.40 ±0.29 | –54.50 ±9.11 | –34.33 ±20.12 | –26.96 ±0.70 |
| ΔGSOLV (kcal/mol) | 36.34 ±0.21 | 32.47 ±6.08 | 15.58 ±9.29 | 8.12 ±0.54 |
| ΔGBIND (kcal/mol) | –23.06 ±0.15 | –22.03 ±5.42 | –18.75 ±12.10 | –18.84 ±0.17 |

The binding affinity of compound BP-1 with acetylcholinesterase (AChE, PDB ID: 1EVE) and Amyloid beta peptide (Aβ1–42, PDB ID: 1IYT) was estimated using the MM/GBSA method on the last 50 ns of molecular dynamics trajectories, sampled at 50 ps intervals (Table 1). Compound BP-1 exhibited a favorable binding free energy with AChE (ΔGBIND = –23.06±0.15 kcal/mol) and Aβ1–42 (ΔGBIND = –18.84±0.17 kcal/mol), indicating stable complex formation in both cases. Among the energy terms, van der Waals interactions dominated the binding stability with values of –44.28±0.19 kcal/mol and –16.92±0.38 kcal/mol for 1EVE and 1IYT complexes, respectively. Electrostatic contributions were also significant, particularly for AChE (–15.12±0.22 kcal/mol). For comparison, standard AChE inhibitors Donepezil and galantamine showed ΔGBIND values of –22.03±5.42 kcal/mol and –18.75±12.10 kcal/mol, respectively, underlining the comparable binding efficiency of compound BP-1. To investigate the spatial stability and binding interactions of the selected compound, we performed binding free energy decomposition analysis for both AChE-1 and $A\beta_{1–42}$-1 complexes. The per-residue free energy contributions are depicted in Fig. 4 and Fig. 5, respectively. These decomposition profiles reveal that several

hydrophobic and aromatic residues performance a critical role in calming the ligand within the binding pocket. Notably, residues such as PHE, TYR, and TRP exhibited substantial negative energy contributions, indicating energetically favorable interactions and strong ligand affinity. These findings suggest that the compound forms stable interactions with key residues through hydrophobic contacts, π-π stacking, and possibly hydrogen bonding, thereby enhancing the overall binding stability during the course of the molecular dynamics simulation. Such interactions are essential for the compound's sustained engagement with the target proteins and may contribute significantly to its inhibitory potential.

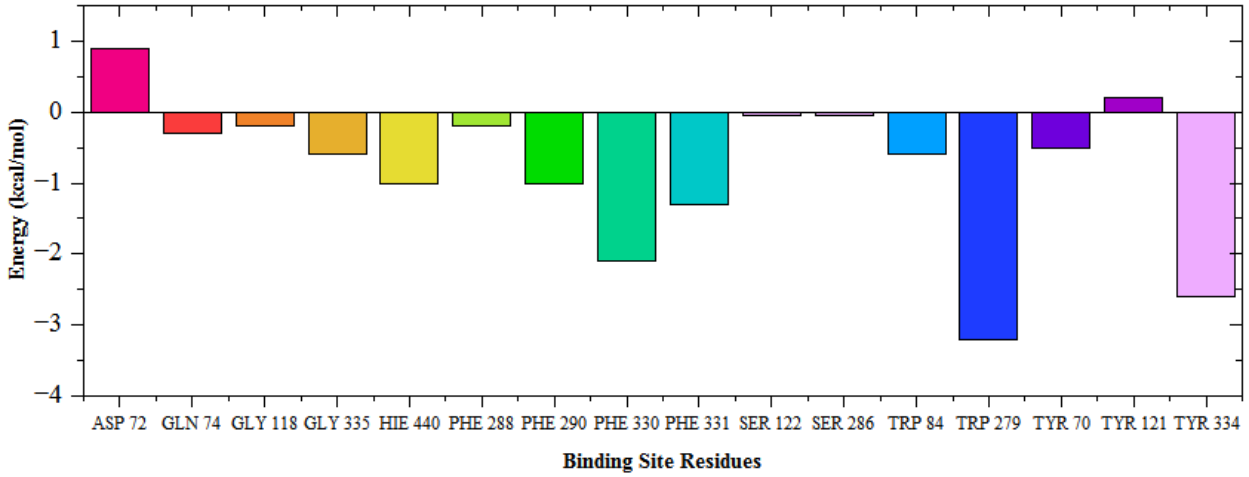


**Fig. 4 Binding free energy decomposition of AChE-1 complex, illustrating the contribution of individual active site residues (in kcal/mol) to the stabilization of the ligand during molecular dynamics simulation**

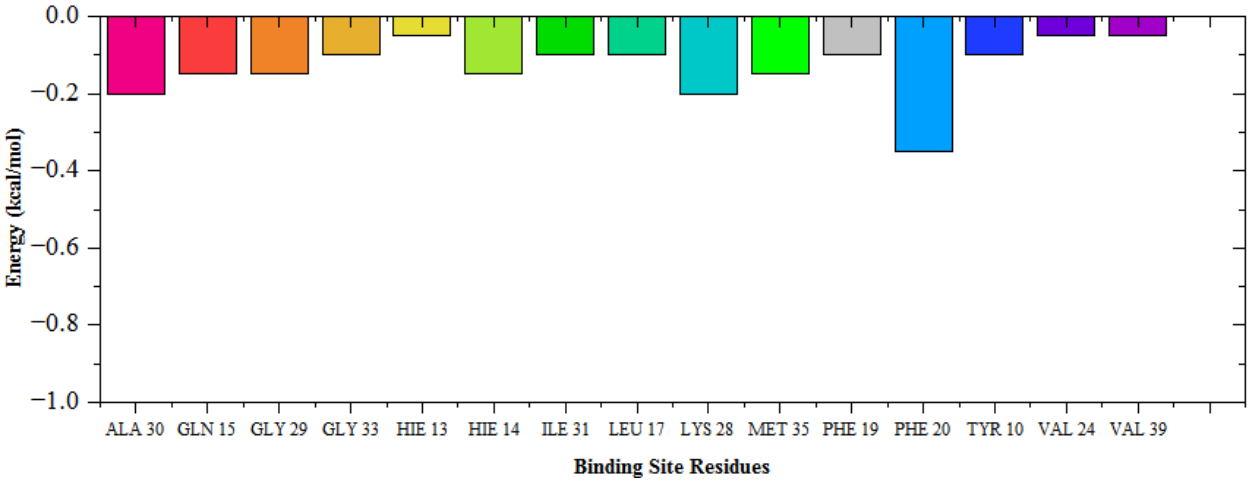


**Fig. 5 Binding free energy decomposition of $A\beta_{1-42}$-1 complex, showing the per-residue energy contributions (in kcal/mol) of the active site residues in stabilizing the ligand throughout the simulation**

**Table 2 Physicochemical properties and BBB permeability**

| Parameter | BP-1 | Donepezil | Galantamine |
|---|---|---|---|
| QPlogPo/w | 1.26 | 4.37 | 2.21 |
| MW (g/mol) | 431.5 | 379.49 | 287.35 |
| SASA (Å²) | 715.8 | 711.8 | 509.8 |
| FOSA (Å²) | 256.1 | 412.5 | 366.1 |
| FISA (Å²) | 141.6 | 44.7 | 58 |
| PISA (Å²) | 278.6 | 254.7 | 85.7 |

| | | | |
|---|---|---|---|
| PSA (Å²) | 99 | 44.7 | 43.5 |
| QPlogBB | −0.71 | 0.13 | 0.34 |

Physicochemical and blood–brain barrier (BBB) permeability assessment for the compound BP-1 were conducted by the QikProp element of the Schrödinger Suite (Table 2). The analysis revealed that BP-1 exhibits favorable drug-like properties with QPlogPo/w of 1.26 and molecular weight of 431.5 g/mol, which are within ranges for CNS-active compounds. The compound also showed a total solvent-accessible surface area (SASA) of 715.8 Å², with contributions from hydrophobic (FOSA = 256.1 Å²), hydrophilic (FISA = 141.6 Å²), and π-system-associated (PISA = 278.6 Å²) components. The polar surface area (PSA) is key indicator for CNS penetration, was calculated to be 99.0 Å² — slightly above the optimal range but still consistent with compounds capable of crossing the BBB. Importantly, the QPlogBB value of BP-1 was predicted as −0.71, indicating moderate to good BBB permeability. For comparison, the standard drug Donepezil showed a QPlogBB of 0.13 and PSA of 44.7 Å², while Galantamine exhibited a QPlogBB of 0.34 and PSA of 43.5 Å². Although BP-1 has higher PSA, its overall balance of physicochemical properties suggests pharmacokinetic profile for essential nervous system targeting. To calculate the inhibitory effect of compound BB-1 on Aβ1–42 fibril formation, TEM analysis was completed. As illustrated in Fig. 6, the TEM image of Aβ1–42 alone at 0 h (Fig. 6a) shows no fibril formation, while after 48 h incubation at 37 °C (Fig. 6b), dense, elongated, and mature fibrillar structures were observed, indicating extensive aggregation. However, co-incubation of Aβ1–42 with curcumin (50 µM) resulted in a noticeable reduction in fibril density and thickness (Fig. 6c), demonstrating partial inhibition. Strikingly, the sample containing Aβ1–42 and BB-1 (50 µM) exhibited a significant reduction in aggregate size and density with visible disaggregation of preformed fibrils (Fig. 6d). These morphological observation confirm the potent anti-aggregation property of BB-1, in agreement with results obtained from ThT fluorescence and confocal microscopy assays.

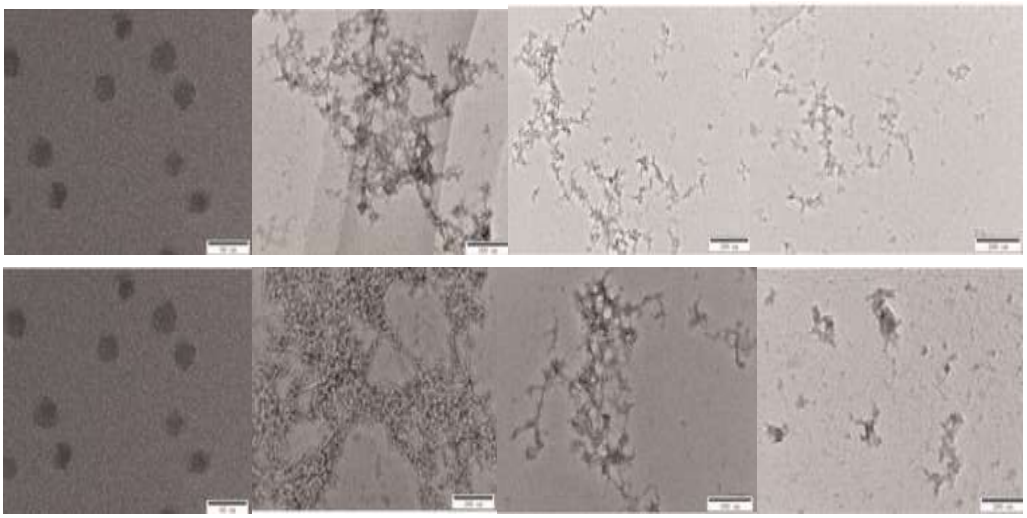

(a) (b) (c) (d)

**Fig. 6 TEM images of $A\beta_{42}$ aggregation inhibition (a) Aβ42 alone (0H) (50µM) (b) Aβ42 alone (48H) (c) $A\beta_{1-42}$ (50µM) and curcumin (50µM) (d) $A\beta_{1-42}$ (50µM) and BB-1 (50µM)**

## 5. CONCLUSION

A series of benzyl Piperazine-based derivatives were computationally designed and estimated as potential multi-target-directed ligands (MTDLs) for the conduct of AD. Among them, compound BP-1 emerged as a promising dual-acting inhibitor, effectively targeting both AChE and $A\beta_{1-42}$ aggregation, the two key pathological hallmarks of AD. Molecular reducing and molecular subtleties imitations demonstrated that BP-1 formed stable and energetically favorable interactions with both AChE (ΔG<sub>BIND</sub> = –23.06 kcal/mol) and $A\beta_{1-42}$ (ΔG<sub>BIND</sub> = –18.84 kcal/mol), surpassing standard drugs such as Donepezil and Galantamine in several binding parameters. Free energy decomposition analyses further confirmed strong interactions with critical residues through hydrophobic contacts and π–π stacking. ADMET and physicochemical evaluations revealed favorable drug-like properties, with moderate blood–brain barrier permeability, suggesting BP-1 as a viable CNS-active candidate. Additionally, TEM analysis confirmed that BP-1 effectively disrupted Aβ fibril formation, exhibiting a more pronounced anti-aggregation effect compared to curcumin. Collectively, these findings strongly support the potential of BP-1 as MTDL scaffold for AD therapy, meriting added in vitro and in vivo validation to establish its therapeutic efficacy

## REFERENCES


[1] Milanifard, M., &Ramezani, M. (2025). Clinical and neurological problems and clinical tests in Alzheimer's patients specializing in Alzheimer's disease. Eurasian Journal of Chemical, Medicinal and Petroleum Research, 4(1), 244-255.

[2] Agustini, D., Sabloak, R., Hasan, S., & Umar, T. P. (2025). The role of fusion proteins as biomarkers and therapeutic agents for Alzheimer's disease: A narrative review. NeuroMarkers, 2(2), 100041.

[3] McGroarty, J., Salinas, S., Evans, H., Jimenez, B., Tran, V., Kadavakollu, S., ...&Atluri, V. (2025). Inflammasome-Mediated Neuroinflammation: A Key Driver in Alzheimer's Disease Pathogenesis. Biomolecules, 15(5), 676.

[4] Yue, Y., Jiang, W., Wang, X., Tian, Z., Cui, Y., & Zhou, X. (2025). Interactions between Oxidative Stress and Mitochondrial Dysfunction in Parkinson's Disease: Potential of Natural Antioxidants. Journal of Biosciences and Medicines, 13(5), 75-99.

[5] Anitha, K., Singh, M. K., Kohat, K., Chenchula, S., Padmavathi, R., Amerneni, L. S., ...& Bhatt, S. (2025). Recent insights into the neurobiology of Alzheimer's disease and advanced treatment strategies. Molecular Neurobiology, 62(2), 2314-2332.

[6] Kadiri, S. K., &Tiwari, P. (2025). Integrating Traditional Medicine with Network Pharmacology for Alzheimer's Treatment. Health Sciences Review, 100223.

[7] Fatima, R., Khan, Y., Maqbool, M., Ramalingam, P. S., Khan, M. G., Bisht, A. S., &Hussain, M. S. (2025). Amyloid-β Clearance with Monoclonal Antibodies: Transforming Alzheimer's Treatment. Current Protein & Peptide Science.

[8] Jojo, G. M., Johnson, J., Kuppusamy, G., & Karri, V. V. S. R. (2025). Alzheimer's Disease: Epidemiology, Etiology, Risk Factors, and Future Predictions. In Multi-Factorial Approach as a Therapeutic Strategy for the Management of Alzheimer's Disease (pp. 41-58). Singapore: Springer Nature Singapore.

[9] Yuan, Y., Yu, L., Bi, C., Huang, L., Su, B., Nie, J., ...& Li, Y. (2025). A new paradigm for drug discovery in the treatment of complex diseases: drug discovery and optimization. Chinese Medicine, 20(1), 40.

[10] Turgutalp, B., & Kizil, C. (2024). Multi-target drugs for Alzheimer's disease. Trends in Pharmacological Sciences.

[11] Niazi, S. K., Magoola, M., & Mariam, Z. (2024). Synergistic Approaches in Neurodegenerative Therapeutics: Multi-Target Drug Innovative Interventions for Alzheimer's Disease. Pharmaceuticals, 17, 741.

[12] Deb, D., Dhanawat, M., Bhushan, B., Pachuau, L., & Das, N. (2025). Targeting Neurodegeneration: The Emerging Role of Hybrid Drugs. Current Drug Targets, 26(6), 410-434.

[13] Verma, A. K., Singh, K., Gupta, J. K., Kumar, S., & Jain, D. (2025). Pharmacological Approaches and Innovative Strategies for Individualized Patient Care. Recent Patents on Biotechnology.

[14] Cummings, J. L., Teunissen, C. E., Fiske, B. K., Le Ber, I., Wildsmith, K. R., Schöll, M., ... &Scheltens, P. (2025). Biomarker-guided decision making in clinical drug development for neurodegenerative disorders. Nature Reviews Drug Discovery, 1-21.

[15] Wang, Y., Lei, M., Zhao, Z., Wu, S., Zheng, X., Qiao, H., & Yang, X. (2025). Multi-targeted pharmacological properties of cinnamylpiperazine derivatives: a comprehensive review. Medicinal Chemistry Research, 34(1), 19-44.

[16] Almehmadi, M., Allahyani, M., Alsaiari, A. A., Asif, M., & Kumar, S. (2025). Neuropharmacological Potential of Different Piperazine Analogs: A Recent Prospective. Mini-Reviews in Organic Chemistry, 22(1), 65-84.

[17] Swati, Raza, A., Singh, B., &Wadhwa, P. (2025). Novel Aromatic Heterocycles for Dual MAO A and B Inhibitors: A Promising Strategy for Parkinson's Disease Treatment. ChemistrySelect, 10(1), e202404978.

[18] Ravikumar, B., Cichońska, A., Sahni, N., Aittokallio, T., &Rahman, R. (2025). Advancements in Rational Multi-Targeted Drug Discovery: Improving the Efficacy-Safety Balance of Small Molecule Cancer Therapeutics. Polypharmacology: Strategies for Multi-Target Drug Discovery, 109-125.

[19] Liu, X., Li, Q., Yan, X., Wang, L., Qiu, J., Yao, X., & Liu, H. (2025). A Specialized and Enhanced Deep Generation Model for Active Molecular Design Targeting Kinases Guided by Affinity Prediction Models and Reinforcement Learning. Journal of Chemical Information and Modeling, 65(7), 3294-3308.

[20] Vemulapalli, S. (2025). Targeting intrinsically disordered proteins (IDPs) in drug discovery: opportunities and challenges. Computational Methods for Rational Drug Design, 493-517.

[21] Takomthong, P., Waiwut, P., &Boonyarat, C. (2025). Targeting multiple pathways with virtual screening to identify the multi-target agent for Alzheimer's disease treatment. Journal of Computer-Aided Molecular Design, 39(1), 1-12.

[22] Zhang, Z., Luo, G., Ma, Y., Wu, Z., Peng, S., Chen, S., & Wu, Y. (2025). GraphkmerDTA: integrating local sequence patterns and topological information for drug-target binding affinity prediction and applications in multi-target anti-Alzheimer's drug discovery. Molecular Diversity, 1-18.

[23] Huang, C., Liu, Y., Wang, S., Xia, J., Hu, D., &Xu, R. (2025). From Genes to Metabolites: HSP90B1's Role in Alzheimer's Disease and Potential for Therapeutic Intervention. NeuroMolecular Medicine, 27(1), 6.

[24] Leal, C. B. Q., Zimmer, C. G., Sinatti, V. V., Soares, E. S., Poppe, B., de Wiart, A. C., ... &Bottos, R. M. (2024). Effects of the therapeutic correction of U1 snRNP complex on Alzheimer's disease. Scientific Reports, 14(1), 1-17.

[25] Qin, G., Song, R., Sun, J., Chen, B., Liu, Z., Han, L., ...& Li, C. (2025). Investigating the therapeutic effects of Shenzhiling oral liquid on Alzheimer's disease: a network pharmacology and experimental approach. 3 Biotech, 15(1), 14.

[26] Wang, F., Wang, J., Chen, T., Wang, S., Meng, X., Shen, Y., &Xu, X. (2025). Systematic Identification of Mitochondrial Signatures in Alzheimer's Disease and Inflammatory Bowel Disease. Molecular Neurobiology, 1-31.

[27] Tran, T. S., & Tran, T. D. (2025). Flavonoid carbamate hybrids: design, synthesis, and evaluation as multi-target enzyme inhibitors for Alzheimer's disease. RSC advances, 15(21), 16855-16868.

[28] Wang, Y., Yan, C., Qi, Y., Zhao, R., Wan, Y., Lyu, Z., ...& Shi, J. (2025). Harnessing multi-target nanosweepers inhibiting β-amyloid aggregation, scavenging reactive oxygen species and overcoming the blood brain barrier for rescuing Alzheimer's disease. Chemical Engineering Journal, 508, 161138.

[29] Khoba, K., Kumar, S., &Purty, R. S. (2025). In silico analysis of Chlorophytumborivilianumphytocompounds as a multi-targeted directed ligand (MTDL) against type 2 diabetes mellitus-induced Alzheimer's disease. Natural Product Research, 1-7.

[30] Du, B., Zou, Q., Wang, X., Wang, H., Yang, X., Wang, Q., & Wang, K. (2025). Multi-targeted Engineered Hybrid Exosomes as Aβ Nanoscavengers and Inflammatory Modulators for Multi-pathway Intervention in Alzheimer's Disease. Biomaterials, 123403.

[31] Wang, N.M., Shi, L., Liu, Y.B., Zhang, X.L., Yu, L.Q., Shen, S.G. and Lv, Y.K., 2025. Interaction Mechanism Between Andrographolide and α-Glucosidase: Multispectroscopy and Molecular Docking Analyses. Luminescence, 40(6), p.e70206.

[32] Ihsan, M., Din, F., Zamli, K.Z., Ghadi, Y.Y., Alahmadi, T.J. and Innab, N., 2025. A modified grey wolf optimizer with multi-solution crossover integration algorithm for feature selection. Journal of Ambient Intelligence and Humanized Computing, pp.1-17.

[33] Farhangmehr, V., Imanian, H., Mohammadian, A., Cobo, J.H., Shirkhani, H. and Payeur, P., 2025. A spatiotemporal CNN-LSTM deep learning model for predicting soil temperature in diverse large-scale regional climates. Science of The Total Environment, 968, p.178901.

[34] Yadav, L.K., Raviraju, G., Kumar, Y., Lodhi, V.K., Sarkar, S.S. and Kumar, V., 2025. Ellman's reagent for specific turn-on chromogenic detection and differentiation of nerve agents: A platform for enzyme-free approach. Microchemical Journal, 212, p.113298.

[35] Mari, C. and Mari, E., 2025. Stochastic DNN-based models meet hidden Markov models: A challenge on natural gas prices at the Henry Hub. Neural Computing and Applications, pp.1-20